Long baseline imaging with LOFAR

Javier Moldón and Eskil Varenius

1 Introduction

The prime reason to use long baselines is to obtain very high-resolution images. Using the longest LOFAR baselines, subarcsecond imaging is possible in the HBA band and the upper part of the LBA band. Early science results include detailed images of quasar jets, and imaging of individual supernova remnants in M82. In this chapter we describe calibration and imaging of international LOFAR stations. The Very Long Baseline Interferometry (VLBI) techniques are explained, as well as the different steps required to properly calibrate the international stations. Some of the discussions will be focused on the LOFAR HBA; calibration and imaging of long baseline data from LBA stations is more challenging and still need additional testing and optimization.

2 International LOFAR stations

The majority of the LOFAR stations, namely the core and remote stations, are distributed over an area roughly 180 km in diameter predominantly in the northeastern Dutch province of Drenthe. Currently, the array also includes 8 international LOFAR stations across Europe that provide maximum baselines up to 1292 km. One additional station is planned to be completed in Hamburg (Germany) in 2014, and three stations in Poland will commence construction in 2014, extending the maxi-

Javier Moldón
ASTRON, Postbus 2, 7990 AA Dwingeloo, The Netherlands, e-mail: moldon@astron.nl

Eskil Varenius
Onsala Space Observatory, Dept. of Earth and Space Sciences, Chalmers University of Technology, SE-43992 Onsala, Sweden e-mail: varenius@chalmers.se

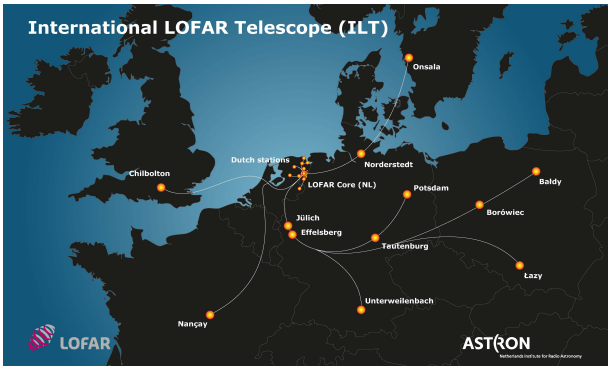

Fig. 1 LOFAR is composed by 24 core stations and 13 remote stations in the Netherlands, and 8 (+4 planned) international stations.

mum baseline to ∼2000 km. Fig. 1 shows the distribution of current and planned stations of International LOFAR.

Observations with the LOFAR international stations are mainly different from the Dutch array observations in that station separations above 200 km provide different scales that require different approaches. The main differences in the array itself are that the density of stations is scarce, and provides a less dense uv-coverage, that the instrument has a reduced field of view (FoV), and that the atmospheric conditions above each station are highly uncorrelated, making the phase calibration much more delicate.

2.1 uv-coverage

The maximum baseline of an interferometer determines the spatial resolution of the instrument. The core stations provide maximum baselines of 2.7 km, the remote stations up to 120 km, and the international stations of 1300 km. Table 1 shows the distances between each pair of international stations, and CS001 as a reference of the location of the center of the array. However, the density of visibilities in the *uv* space determines the fidelity of the image. The LOFAR core provides a very dense *uv* sampling, but at the longest *uv* distances it is much more scarce. A typical LOFAR *uv* coverage is shown in Fig. 2. We can see that the sampling covers 3 orders of magnitude in *uv* distance.

	CS001	DE601	DE602	DE603	DE604	DE605	FR606	SE607	UK608
CS001	0	266	581	396	419	226	700	594	602
DE601	266	0	390	344	476	53	490	833	590
DE602	581	390	0	277	455	440	690	990	959
DE603	396	344	277	0	186	372	800	714	920
DE604	419	476	455	186	0	487	957	556	1005
DE605	226	53	440	372	487	0	498	807	552
FR606	700	490	690	800	957	498	0	1292	495
SE607	594	833	990	714	556	807	1292	0	1110
UK608	602	590	959	920	1005	552	495	1110	0

Table 1 Separation in km between the main core and the currently available international stations.

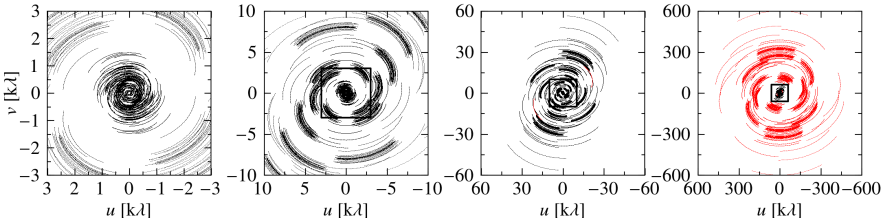

Fig. 2 *uv* coverage for a typical 4-hr observation of a source at declination +48° with a single subband centred at 140 MHz. Only one visibility every 160 seconds is shown. The rectangles in the last three panels show the area covered by the previous panel. Visibilities corresponding to baselines with international stations are plotted in red.

2.2 Field of view (FoV) and averaging

The area possible to image in a single LOFAR observation (NL or international) is limited by several factors such as the station beam, geometrical/projection effects, W-projection artefacts, variations in the atmosphere within the image, and averaging of visibility data, also referred to as time and frequency *smearing*. The latter is mainly important for long baselines and in this section we describe this effect in more detail.

Since correlators output a discrete set of visibilities (i.e. samples in time and frequency), averaging is to some extent always done on interferometric data. We may also average the data further after correlation to reduce the computational resources needed for calibration and imaging. Any averaging must however be done with care. Averaging a range of samples in time and frequency together corresponds to averaging over a small parallelogram in Fourier space. This means some information is lost, and one has to take care to not lose information that could affect the scientific results. For LOFAR, the standard *raw* data are delivered from the correlator with resolution 1 second in time, and 64/channels per subband. Each subband (using the standard 200 MHz clock) is 195 kHz wide, meaning that the default minimum averaging bandwidth is 3 kHz. This will limit the dynamic range at some distance from the observed phase center, similar to the station beam effects described above.

A detailed description of the averaging losses is beyond the scope of this chapter, we merely quote the often used results by Taylor et al. (1999) chapter 18, who derived two expressions to estimate the average amplitude loss due to averaging in frequency and time, at some distance from the phase center. For frequency smearing, we can use their expression 18-24 assuming a square bandpass and circular Gaussian tapering, where the reduction in amplitude can be estimated as

$$\frac{I}{I_0} = \frac{\sqrt{\pi}}{2\sqrt{\ln 2}} \frac{\theta \nu_c}{r \Delta \nu} \mathrm{erf}\left(\sqrt{\ln 2} \frac{r \Delta \nu}{\theta \nu_c} \right) \quad (1)$$

where θ is the synthesized beam size (FWHM), ν_c is the central frequency of the observation, r is the distance from the phase center, and $\Delta \nu$ is the bandwidth. Note that the units of θ and r cancel if they are given in the same unit. Note also that this expression is in fact independent of central frequency ν_c since the synthesised beam also scales with ν_c, only the bandwidth is important.

For time smearing, we may use their formula 18-43, assuming a 12 hour average over a circular UV-coverage with Gaussian tapering:

$$\frac{I}{I_0} = 1 - 1.22 \times 10^{-9} \left(\frac{r}{\theta} \right)^2 \tau_a^2 \quad (2)$$

where τ_a is the averaging time in seconds.

What loss to define as acceptable of course depends on your science, in particular the brightness of your target, but as a general guide one may tolerate 5% loss in amplitude due to averaging. Using the standard LOFAR raw data values, we have calculated the corresponding circle (diameter, to compare with station FWHM) for different observing frequencies, see Table 2. We note that, except for the lowest LBA frequencies, we are limited by time averaging, where the 5% loss diameter is smaller than the station beam. Note that this limitation is not present for shorter baselines, and usually not a cause for worry in NL-LOFAR observations. But, with the longest baselines, the main restriction may (if you need excellent sensitivity) be the averaging by the raw data.

2.3 Differential delay: cause and effects

The interferometric phase depends on the time delay of the signal to reach two different stations. In particular, the phase delay is $\tau_\phi = \frac{\phi}{2\pi\nu}$. This means that at low frequencies, a small change in τ_ϕ produces a fast change in phase. We note that, since the phases are always relative to a reference station, the delay contribution comes from the differential delay affecting two stations. The delay depends on the geometry of the stations with respect to the observed source (geometric delay), instrumental effects (instrumental delay), and propagation of the signal through the atmosphere (ionospheric delay). If the model applied at correlation time were perfect, all stations would see a delay offset of zero for all sources, but deviations are produced by several factors. First, errors in station positions (and currently in a

Freq. (MHz)	λ (m)	Int. PSF FWHM ($''$)	Int. station FHWM (deg)	5% loss, 1s Diam. (deg)	5% loss, 64ch/SB Diam. (deg)
15	19.99	3.30	19.39	11.73	4.29
30	9.99	1.65	9.70	5.86	4.29
45	6.66	1.10	6.46	3.91	4.29
60	5.00	0.82	4.85	2.93	4.29
75	4.00	0.66	3.88	2.35	4.29
120	2.50	0.41	2.59	1.47	4.29
150	2.00	0.33	2.07	1.17	4.29
180	1.67	0.27	1.73	0.98	4.29
200	1.50	0.25	1.55	0.88	4.29
210	1.43	0.24	1.48	0.84	4.29
240	1.25	0.21	1.29	0.73	4.29

Table 2 Station FWHM Values taken from (van Haarlem et al. 2013, App. B). Loss due to time- and frequency averaging as calculated using eqns. 2 and 1. Note that the expression given for frequency smearing is in fact independent of central frequency since the synthesised beam also scales with frequency, only the bandwidth is important.

much lower level errors in the the Earth orientation parameters, EOPs) used by the correlator produce variability of about $\pm$75 ns with a 24 h periodicity. The current correlator model used by LOFAR is insufficiently accurate, and this source of error can be expected to be greatly reduced in the near future. Instabilities in the rubidium clocks can produce delay rates up to 20 ns per 20 min, which corresponds to about a radian per minute at 150 MHz (van Haarlem et al. 2013). In total, non-dispersive instrumental delays of up to $\sim$ 100 ns and delay rates of up to $\sim$20 ns h^{-1} are expected. Second, for any given source, errors in the *a priori* centroid position (for example from low-frequency catalogues, with a typical error of a few arcseconds) and/or extended structure on subarcsecond scales contribute an additional delay offset. The maximum baseline between an international station and the LOFAR core is 700 km (see Table 1); a positional error of $1.5''$ will lead to a delay error of $\sim$15 ns on this baseline.

The ionospheric contribution to the delay changes as a function of time, position, and zenith angle. The magnitude of the changes depend on the Total Electron Content (TEC) of the ionosphere, with a delay of $\tau_{\rm ion} = c^2 r_{\rm e}/(2\pi\nu^2) \times$ TEC, being c the speed of light, $r_{\rm e}$ the classical electron radius, and ν the observed frequency, and TEC is usually measured in TEC Units (1TECU $= 10^{16}$ electrons m^{-2}). The TEC can can be estimated using models derived from observations of GPS satellites. Models are available from different institutes, such as the Jet Propulsion Laboratory (JPL), the Center for Orbit Determination in Europe (CODE), the ESOC Ionosphere Monitoring Facility (ESA), or the Royal Observatory of Belgium GNSS, among others. The models contain information on the vertical total electron content (VTEC) during an observations. We note that the TEC values above the stations are a lower limit of the slant ionospheric contribution that depends on the source elevation at each station. More details can be found in, for instance, Nigl et al. (2007) and Sotomayor-Beltran et al. (2013).

Although the VTEC follows a 24-h trend strongly correlated with the Sun elevation, the short-term (10–60 minute) variations between the widely separated international stations are virtually uncorrelated. The ionospheric contribution typically dominates the total delay and delay rate for international LOFAR stations. We have used VLBI observations (VLBA project code BD152) at 300 MHz, or 1 m wavelength, of bright and compact pulsars at different angular separations to obtain a rough estimate of the delay difference between sources separated 1–5 degrees at elevations of 50–80°. As a first approximation we estimated that the dispersive delay difference between sources at different lines of sight should be about 5 ns per degree of separation, for a source elevation of 60°.

Noise is the final contribution to the delay offset, and depends on the brightness of the source and the sensitivity of the station. In summary, in a normal observation phase uncertainties are cause by source position and structure errors, differential ionosphere, uncorrected instrumental delays, and noise. Table 3 summarises the main contributions and the time scale in which they change.

Table 3 Approximate delay contributions at 140 MHz to a 700 km baseline.

Effect	Delay	Time scale
Non-Dispersive		
Correlator model error	$\sim$ 75 ns	24h (periodic)
Station clocks	$\sim$ 20 ns	$\sim$20 min
Source position offset (1.5″)	$\sim$ 15 ns	–
Dispersive		
Slowly varying ionosphere	$\sim$ 300 ns	$\sim$hours
Rapidly varying ionosphere	$\gtrsim$10 ns	$\sim$ 10 min
Differential ionosphere (source elevation 60 deg)	5 ns/deg sep.	–

3 Long baseline calibration

Calibration of these long baselines poses a special challenge compared to LOFAR observations with the Dutch array, and these can be addressed using tools developed for cm wavelength VLBI. The calibration process must derive the station-based amplitude and phase corrections in the direction of the target source with adequate accuracy as a function of time.

3.1 Phase calibration

Due to the large and time-variable delay offsets at each station, solving for phase corrections directly (approximating the correction as constant over a given solu-

tion time and bandwidth) would require very narrow solution intervals for VLBI, and hence an extremely bright calibrator source. However, such a source would be unlikely to be close on the sky to the target, with a separation of perhaps tens of degrees, and the differential atmosphere/ionosphere between the calibrator and the target direction would render the derived calibration useless in the target direction. In order to make use of calibrators closer to the target, VLBI calibration therefore solves for 3 parameters (phase, non-dispersive delay, and phase rate) in each solution interval, allowing the solution duration and bandwidth to be greatly extended. This approach makes a number of assumptions:

1. The change of the delay resulting from the dispersion is negligible, so the total delay can be approximated as a constant across the solution bandwidth;
2. The change in delay over the solution time can be approximated in a linear fashion;
3. The change in phase over the solution bandwidth due to the change in delay over the solution time is small (since the time variation is approximated with a phase rate, rather than a delay rate).

Meeting these assumptions requires that the solution interval and bandwidth be kept relatively small, which is at odds with the desire to maximise sensitivity, which demands that the solution interval and bandwidth be as large as possible.

For 110–240 MHz (LOFAR High Band) observations on long baselines, the approximations made when solving for phase, phase rate, and non-dispersive delay fail badly when applied to bandwidths of tens of MHz or more. Two options present themselves: to add additional parameters (covering dispersive delay and dispersive delay rate) to the global fit, or to reduce the solution bandwidth such that the constant dispersive delay approximation becomes valid again. The former option is obviously preferable from a sensitivity perspective, but greatly expands and complicates the solution search space. Efforts are underway to implement such an expanded fit, including in addition differential Faraday rotation, which becomes increasingly important at frequencies below 100 MHz. First tests on individual long baselines of LOFAR as well as baselines to other telescopes are promising, but the algorithms are not yet sufficiently mature for automatic calibration. Accordingly, we focus here on sources which can serve as primary calibrators under the latter set of conditions, where solution bandwidths are limited to no more than a few MHz.

The system equivalent flux density (SEFD) of a single LOFAR core station is approximately 1500 Jy[1] at a frequency of $\sim$140 MHz (van Haarlem et al. 2013). An international station has twice the collecting area of a core station at $\sim$140 MHz, so the expected SEFD is around 750 Jy. The 24 core stations can be coherently combined into a single phased array with an SEFD of $\sim$65 Jy, in the absence of correlated noise (i.e., when the observed field only contains sources significantly fainter than the station SEFD). The theoretical 1σ baseline sensitivity of an international station to the phased-up core station, given 3 MHz of bandwidth and 4 minutes of observing time, is hence 8 mJy in a single polarisation. A source with a compact

[1] A LOFAR core station consists of two sub-stations (2×24 tiles) in the HBA.

flux density of 50 mJy yields a theoretical baseline signal-to-noise ratio of 6, and is therefore a potential primary calibrator. In the real world, the sensitivity of the phased-up core station will be reduced by failing tiles, imperfect calibration and correlated (astronomical) noise, and so 50 mJy should be considered a lower limit on the useful primary calibrator flux density.

In addition to being sufficiently bright, the primary calibrator must be close enough to the secondary calibrator/target field that the differential delay between the two fields does not lead to decorrelation when phase-only secondary calibration is performed (just as for cm VLBI). The solution bandwidths are narrower by a factor of $\gtrsim$10 than for cm VLBI, which is helpful, but the ionospheric delay (inversely proportional to observing frequency squared) is much greater, meaning that on balance a closer calibrator will be needed than the $\lesssim$5 degrees typical for cm VLBI. The maximum acceptable separation will be a strong function of ionospheric conditions and elevation, but at face value, given a bandwidth 20 times narrower (e.g., 3 MHz vs 64 MHz) and frequency 10 times lower (140 MHz vs 1400 MHz), one would expect that the calibrator would need to be separated by $\lesssim$1 degree. This is borne out by commissioning observations with LOFAR, which have shown acceptable results with separations up to several degrees in favourable ionospheric conditions, and unacceptable results with separations as small as $\sim$0.8 degrees in poor conditions. Ideally, then, a primary calibrator for International LOFAR observations would be located $\lesssim$1 degree from the secondary calibrator/target field to give acceptable calibration under most circumstances. This leads to the one calibration advantage of International LOFAR compared to cm VLBI; since the beam of an International LOFAR station is $\gtrsim$2 degrees across, the primary calibrator will by necessity be observed contemporaneously with the target source.

Currently, no specific LOFAR tools for solving for the phases, delays and rates are available. The best approach is to conduct the phase calibration of an International LOFAR observation with AIPS[2] (Greisen 2003), produced and maintained by NRAO, using the fringe fitting task FRING. More information can be found in Section 4.6.

3.2 Amplitude calibration

The amplitude calibration consists of finding the antenna gain factors that scales the raw response of each antenna to the real flux density measured. These scaling factors can be found calibrating the data with a bright source with known flux density and structure (for example a point-like calibrator). For core and remote stations, one can use, for example bright sources in low frequency catalogs (such as MSSS). However, for International LOFAR that is in general not possible because (1) there is not yet a catalogue of sources, and therefore the structure of bright sources is unknown at this scales (2) the international stations sample only very long *uv* dis-

[2] http://www.aips.nrao.edu/index.shtml

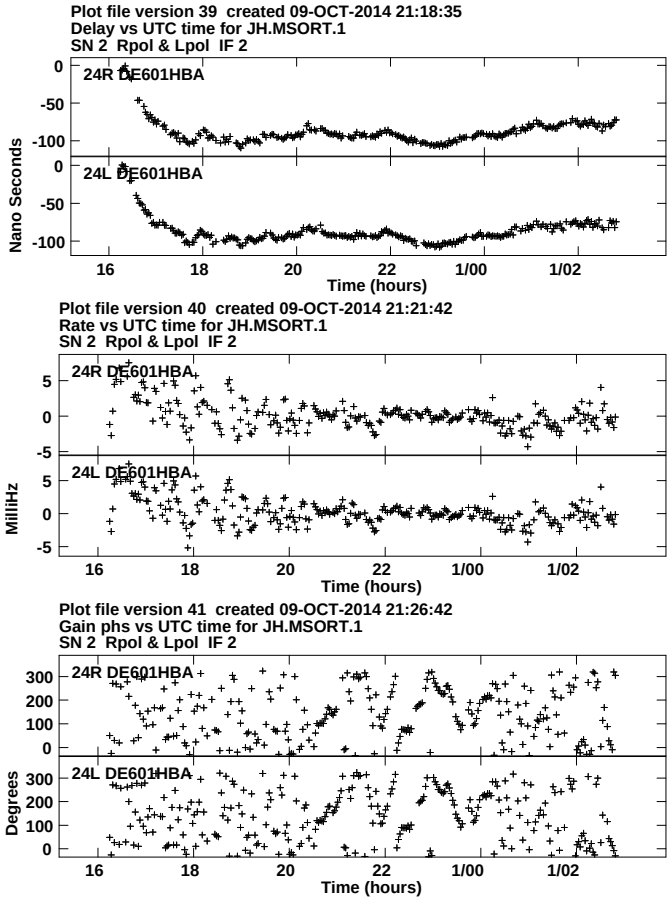

Fig. 3 Delay (top), rate (middle) and phase(bottom) corrections derived for the source J0958+6533 at 154 MHz by FRING for antenna DE601HBA. These plots show the corrections derived for a 10 hour observation (the first segment of project LC0_026). It is clear from the rates and phases that phases changes rapidly during the first and last hours of the experiment. The delay solutions are more stable, although there is a large change in at the start. In general, the ionosphere is more stable during midnight than at sunset or sunrise.

tances (see Fig. 2, right panel) that not overlap with the rest of the array, which can be corrected, and (3) compact and bright regions of potential calibrators, usually AGN, are expected to change with time. In principle, instrumental gains within LOFAR could be tracked with time (this option is currently being commissioning with the COBALT correlator), but since this option is not yet available, making a sufficiently accurate a priori calibration is also not feasible. Therefore, the current approach requires to self-calibrate a bright calibrator to find its small-scale structure, and bootstrap its flux density between the short and long baselines, assuming that the low-resolution flux density of the source is stable and known.

For a science observation, it is recommended to include runs on very a bright and known calibrator (for instance 3C196 or 3C84) and a compact source (for instance a cm-VLBI calibrator or a bright pulsar) to set the amplitude scale, and link the short/long-baselines flux density, respectively. We note that a proper amplitude calibration requires also a good model of the spectral index of the reference calibrator.

4 Practical considerations

4.1 Shift+average

Given the high resolution obtained with the International LOFAR observations, imaging of the region restricted by the time and frequency average of the data with the long-baseline resolution (see Table 2), would require high would require a very high computational cost. If one is interested in multiple objects within the station beam, one needs to phase-shift (and re-project) the *uv*-data to each object before averaging. After correlation, the full-resolution visibility dataset can be shifted and averaged multiple times, to the positions of all the target sources and possibly to one or more nearby calibrators. Starting during cycle three, it will be possible to request shifting and averaging of data to multiple phase centers within a beam as a part of a normal observation.

4.2 Distributing bandwidth on different sources

It is possible to distribute LOFAR bandwidth over a number of beams to simultaneously observe different regions of the sky. In particular, it is possible to divide the bandwidth on target(s) and calibrator, which provides a continuous source calibration without the need of regularly nodding from target to calibrator. Another possibility is to distribute the bandwidth among a large number of sources to search for suitable calibrations. For example one can generate 30 beams to observe simultaneously 30 sources with 3 MHz bandwith as a fast way to search for suitable calibrators (see i.e. Moldon & et al. 2014)

To optimize the observation it is possible to use fewer subbands on the calibrator, and thereby get more subbands, i.e. lower continuum noise, on the target beam. To use fringe finding, we need to sample accurately the residual delay/rate slope (and possibly curvature at low frequencies) present in the data. This can be done with sparse sampling in frequency, where the optimal coverage is achieved by spreading the subbands as a powerlaw density with denser placement of subbands at lower frequencies. The advantage of this approach is that more bandwidth can be placed on the target. The disadvantage is that the calibration becomes a bit more demanding. One reason for this is that the UVFITS format used by AIPS (for running fringe

fitting) requires data in all channels. If we do not have contigouse subband coverage in frequency, we need to insert fake data and flag that (e.g. using NDPPP, see [**Ref. to imaging cookbook?]) before reading the data into AIPS. This will cause an increase in data volume which will slow down processing. Also, spreading the subbands sparsely is always a risk in case your calibrator is weaker than you think. A detailed discussion can be found in Martí-Vidal (2010). The authors analyse how to distribute subbands specifically for LOFAR observations for optimal fringe detection.

4.3 Form a combined station

The huge difference between the *uv* distances provided by core-core baselines and international baselines makes it very difficult to produce images were the very compact and the very diffuse emission can be analysed. When studying the compact structure of a source, the shortest baselines do not add too much information, whereas they difficult the calibration, for example because they are sensitive to a much bigger area of the sky, potentially including hundreds of bright sources up to several degrees away. The core stations can be added to form a coherent "tied station" (TS001) that keeps the core sensitivity and the long baselines to the international stations. Since the core stations share the same clock and are under similar atmospheric conditions, only slow changes in their amplitudes and phases are expected, and thus they can be calibrated by observing a bright primary calibrator once every ~ 1 hr. TS001 is formed by summing baseline visibilities with the NDPPP task "StationAdder". After this step, all original visibilities with core-core baselines can be discarded using the NDPPP task "Filter" to significantly reduce the data volume.

One important benefit of having a tied station is that it works as a very sensitive station. This tied-array station aids in the derivation of calibration solutions to the international stations with FRING, and can be used as a reference station. In Fig. 4 we show calibrated amplitudes and phases for some baselines from some remote stations to a single core station and to the tied station formed by coherently combining 23 core stations. **Note:** A tied-station formed by adding the whole core has a very small (5% amplitude loss at $30''$ distance from phase center) field of view. Although this is rarely a problem for deriving FRING solutions, care is needed if using such combined data to image extended objects.

4.4 Linear to circular polarization

Differential Faraday rotation introduces rapid phase changes with frequency into linear polarisation data on long baselines. For long-baseline observations is preferable to work in a circular (R,L) polarisation basis. In this basis, the ionospheric disturbances are transformed from coupled amplitude/phase effects (as in the linear

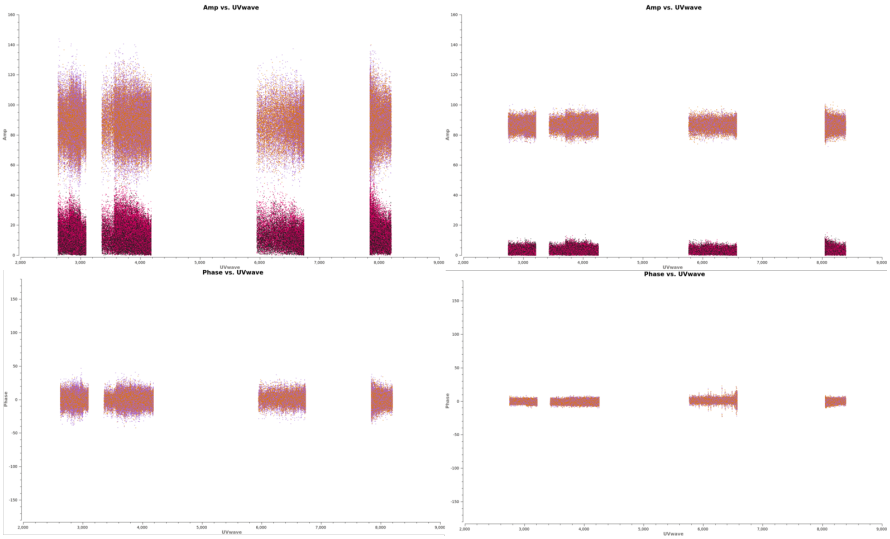

Fig. 4 Amplitude (top) and phase (top) as a function of uv-distance for the baselines between CS001 (left) and TS001 (right) to four remote stations.

X,Y basis) to phase only effects. Since differential Faraday rotation does not mix R and L polarisations we may calibrate RR and LL independently. Furthermore, standard VLBI techniques like fringe fitting work in a circular (R,L) polarisation basis. Therefore, the data have to be converted to circular polarisation before the phase calibration of the long baselines.

Conversion to circular polarisation can be done using the Table Query Language (TAQL) to operate on the measurement set data directly. We note that the effects of the station beam should be calibrated with BBS before converting the data. As the effects of the station beam were already calibrated, this is a simple operation. However, we note that since BBS calibrates the XX and YY components independently, an overall phase-offset between X and Y may remain. Another tool to convert from linear to circular polarisation is *mscorpol*, developed by T. D. Carozzi.

4.5 Convert to UVFITS

Since AIPS understands the UVFITS-format, but not Measurement Sets (MS) we need to convert the data from MS to UVFITS. There are several ways to do this:

- You may use the tool *ms2uvfits* available at the LOFAR cluster, as `ms2uvfits in=[input-MS] out=[output-FITS-file] writesyscal=False`
- You may use the function *exportuvfits* in CASA.

Note that in a UVFITS file there MUST be data for all baselines included, although data can be flagged if baselines are bad. If one tries to reduce data size by exluding particular subarrays with NDPPP one may run into very strange errors in AIPS, since the basic assumptions of UVFITS are not valid. Hence, it is important to ensure that data are contigous in frequency (e.g. by inserting fake data as explained above) and that there are data present for all baselines in the dataset.

The AIPS task FITLD can be used to load the data in to AIPS. For LOFAR data, the parameters digicor=-1 and douvcomp=-1 should be used.

4.6 Brief introduction to calibration tables in AIPS

In AIPS one calibrates data by sucessively finding and improving corrections for the amplitude and phase of visibilites. These corrections are stored in tables. Each correction derived is store in an 'SN' table, and the cumulative corrections are stored in a 'CL' table. The SN table will have a resolution which you specify for each task, i.e. if you find corrections averaging data in two minute chunks, the SN table will have one value every two minutes. The CL table may have a different granularity, so that when applying a specific SN table, you may (automatically) interpolate to CL-table entries between the SN entries. When you are done with calibration, the CL-table including all your corrections can be multiplied with your data using the task SPLIT to produce a UVFITS file with the corrected data.

5 Finding calibrators

Until a good catalogue of compact sources at MHz frequencies is available, it is important to take into account that a science observation might require an preparatory search of calibrators. A fast method using the distribution of bandwidth between many sources (see Sect. 4.2) is described in Moldon & et al. (2014). A preselection based on a number of parameters from existing catalogues, such as the low-frequency spectral index, and the flux, ca be performed to optimize the search. In particular the most useful catalogues are the VLSS, at 74 MHz, 4 m wavelength (Lane et al. 2012), the WENSS catalogue at 325 MHz, 92 cm wavelength (Rengelink et al. 1997), and, specially The Multifrequency Snapshot Sky Survey (MSSS), which comes from LOFAR observations (Heald & LOFAR Collaboration 2014).

Moldon & et al. (2014) showed that a density of ~ 1 good calibrator per square degree based on two fields with Galactic latitudes of $+26.6^\circ$ and $+43.4^\circ$. However, we expect less compact sources at lower Galactic latitudes due to interstellar scattering. The Galactic electron density model NE2001 (Cordes & Lazio 2002) predicts an scattering at a galactic latitude of 50° of almost 100 mas at 150 MHz, which is five times smaller than our resolution. However, the scattering is about

300 mas, similar to our beamsize, at latitudes of 5–10°, depending on the longitude. Therefore, observations below a Galactic latitude of 10° are likely to be affected by scattering on the longest baselines, and the effect should be severe below about 2°, especially towards the Galactic Center.

6 Observing strategy

For cm VLBI, the dispersive delay due to the ionosphere is small (and so are the changes with time), meaning that solution intervals of duration minutes and width tens to hundreds of MHz are generally permissible. After application of the solutions from the primary calibrator, it is common to use a secondary calibrator[3] closer to the target source (separation ∼arcmin), or to use the target source if it is bright enough for "self-calibration", solving only for the phase (no delay or rate). This second phase-only calibration is used to refine the calibration errors that result from the spatial or temporal interpolation of the primary solutions. Because this is a problem with fewer degrees of freedom, lower signal-to-noise ratio (S/N) data can be used. Additionally, because the bulk delay has already been removed, even more bandwidth can be combined in a single solution for a further improvement in S/N. A secondary calibrator can therefore be considerably fainter (usually ∼1-10 mJy versus >100 mJy for a primary calibrator). This typical VLBI calibration strategy is illustrated in Figure 5.

Moldon & et al. (2014) propose the following approach for an International LOFAR observation:

1. Identify candidate primary calibrators up to separations of a few degrees by using any of the criteria discussed in Sect. **??**;
2. Conduct a short observation in snapshot mode as described in Sect. **??** before the science observation to identify the best primary calibrator (or calibrators).
3. If required and time permits, follow up with a "full bandwidth" snapshot observation to identify one or more secondary calibrators;
4. Set up the scientific observation to dwell on the field containing the primary calibrator and the target/secondary calibrator;
5. Include periodic scans (every ∼ hour) on a bright Dutch array calibrator to calibrate the core stations in order to form the tied station.
6. Shift phase centre to primary calibrator, preprocess and obtain delay solutions as described in this paper, apply them to the unshifted dataset;
7. If a secondary calibrator is to be used and is not yet identified, select 10 minutes of data and perform shift/averaging to candidate secondary calibrator sources;
8. If secondary calibrator is used: shift and average primary-calibrated dataset, image and selfcalibrate, apply solutions to the unshifted dataset;
9. Shift and average calibrated dataset, image and (if needed) selfcalibrate target.

[3] A secondary calibrator is often referred to as an "in-beam" calibrator if it is close enough to the target source to be observed contemporaneously

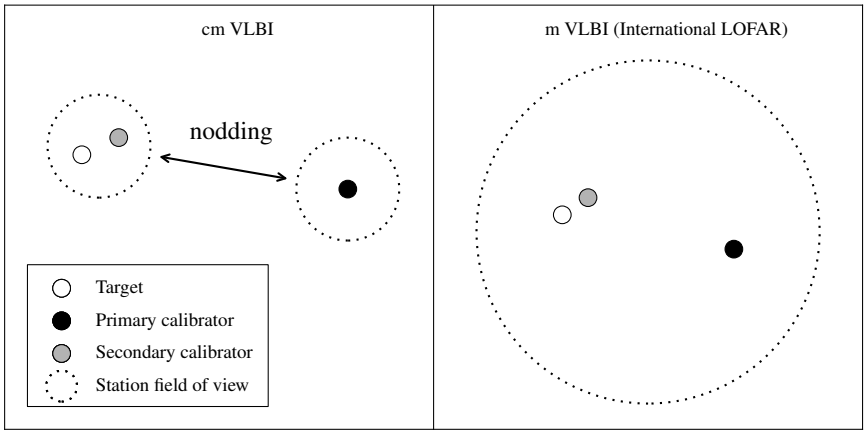

Fig. 5 Typical calibration setup for cm VLBI (left) and International LOFAR (right). Note that in some cases the target may itself function as the secondary calibrator. A secondary calibrator is not always required for cm VLBI, but will almost always be needed for International LOFAR, unless the primary calibrator is fortuitously close. The larger field of view of LOFAR means that both the primary and secondary calibrators will always be observed contemporaneously, unlike in cm VLBI, where nodding between the primary calibrator and target is typically required (shown by the double arrow in the left panel).

In the near future, the pipeline used for this project will be developed, in collaboration with the LOFAR operations team, into an expanded form capable of carrying out the approach described above. This pipeline will be made available to all International LOFAR observers, delivering a reduced data volume for long-baseline observations and enabling calibrated data to be more quickly produced.

Acknowledgements Thanks to people. Other thanks.

AIPS is produced and maintained by the National Radio Astronomy Observatory, a facility of the National Science Foundation operated under cooperative agreement by Associated Universities, Inc.

References

Cordes, J. M. & Lazio, T. J. W. 2002, ArXiv Astrophysics e-prints

Greisen, E. W. 2003, Information Handling in Astronomy - Historical Vistas, 285, 109

Heald, G. & LOFAR Collaboration. 2014, in American Astronomical Society Meeting Abstracts, Vol. 223, American Astronomical Society Meeting Abstracts #223, 236.07

Lane, W. M., Cotton, W. D., Helmboldt, J. F., & Kassim, N. E. 2012, Radio Science, 47, 0

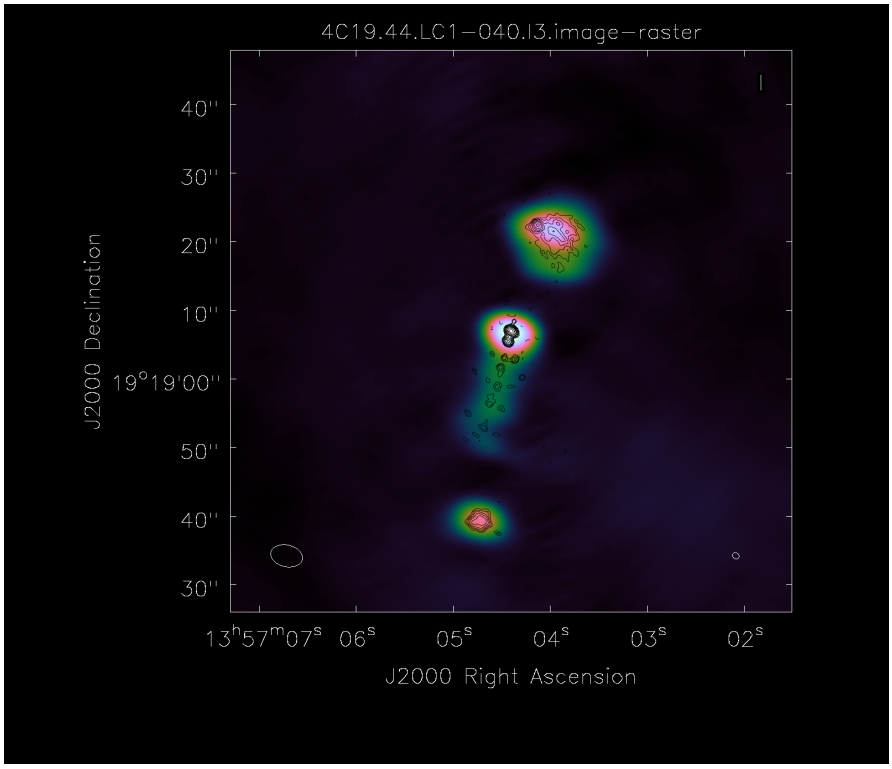

Fig. 6 Example of nice image produced with the long baselines. We have to find something.

Martí-Vidal, I. 2010, A&A, 517, A83
Moldon, J. & et al. 2014, A&A, submitted
Nigl, A., Zarka, P., Kuijpers, J., et al. 2007, A&A, 471, 1099
Rengelink, R. B., Tang, Y., de Bruyn, A. G., et al. 1997, A&AS, 124, 259
Sotomayor-Beltran, C., Sobey, C., Hessels, J. W. T., et al. 2013, A&A, 552, A58
Taylor, G. B., Carilli, C. L., & Perley, R. A., eds. 1999, Astronomical Society of the Pacific Conference Series, Vol. 180, Synthesis Imaging in Radio Astronomy II
van Haarlem, M. P., Wise, M. W., Gunst, A. W., et al. 2013, A&A, 556, A2